

Vision-Based Agile Landing on Turbulent Waters

Dimosthenis Angelis¹, Leonard Bauersfeld², Davide Scaramuzza², Evangelos Boukas¹

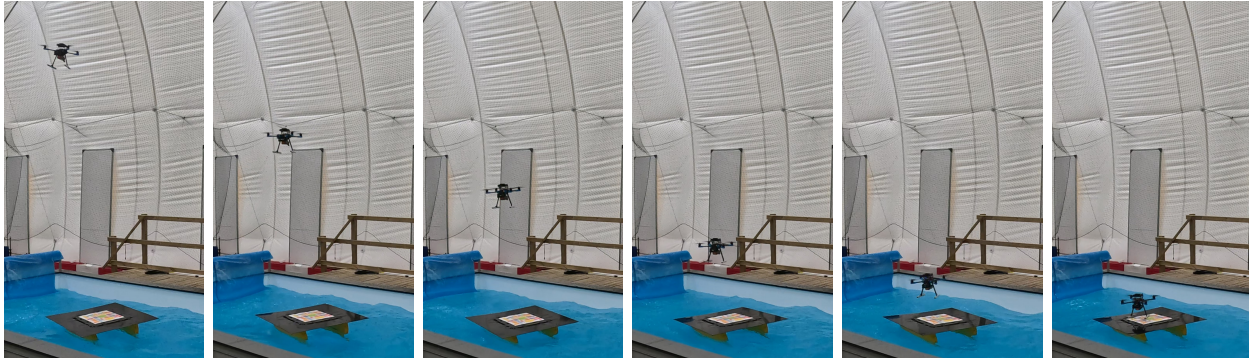


Fig. 1: A quadrotor lands autonomously on a floating platform in a pool subject to manually generated waves. The landing pad uses a randomly generated target, and all sensing and computation are performed onboard.

Abstract—Autonomous landing of Unmanned Aerial Vehicles on maritime vessels is challenging due to the coupled motion of the vehicle and landing platform in open-sea conditions. This paper presents a reinforcement-learning-based approach for autonomous multirotor landing on moving maritime platforms without requiring explicit platform-state information. The proposed method uses multirotor state measurements together with local visual features, consisting of keypoints and associated descriptors extracted from the landing surface, to predict attitude and thrust commands. These commands are tracked by a conventional low-level controller. The policy is trained in simulation using synthetic keypoints with randomly generated normalized descriptors, enabling zero-shot deployment with different local feature extractors onboard the UAV. We evaluate the method in a realistic simulator and show that it outperforms a state-of-the-art Model Predictive Control baseline under platform motions corresponding to “Very Rough” sea conditions. Finally, we perform extensive real-world experiments, demonstrating autonomous onboard landing using two different local feature extractors. To the best of our knowledge, this is the first approach for agile multirotor landing on maritime platforms in turbulent waters that does not rely on an explicit platform-state representation.

Index Terms—Reinforcement Learning, Aerial Systems: Perception and Autonomy, Visual Learning

I. INTRODUCTION

Utilization of Unmanned Aerial Vehicles (UAVs) in maritime operations has increased in recent years due to their effectiveness in search and rescue [1]–[3], wildlife

monitoring [4], and surveillance [5]. Their elevated viewpoint and superior agility, compared to surface vehicles, make them particularly effective for detecting objects on the water surface. However, despite their operational advantages, UAVs are constrained by their limited endurance and often require a carrier surface vehicle to transport them to the area of interest for deployment and recovery. This requirement highlights the need for autonomous, agile landing methods that can support efficient and reliable UAV operations from moving maritime platforms.

The task of landing a multirotor on a 6-Degree-of-Freedom (6-DoF) platform is challenging due to the harsh nature of the sea and the requirements of a successful landing. Traditionally, these missions require the UAV to be able to detect and predict the movement of the landing platform, either directly through cameras that detect predefined geometrical targets on the platform surface, or indirectly by communicating with the landing platform itself. The UAV can then use this information to control its descent and perform the landing. This task becomes increasingly more difficult when the geometric targets are visually degraded due to environmental or operational factors. To the best of our knowledge, no prior approach has demonstrated agile multirotor landing on maritime platforms in turbulent waters without relying on an explicit platform-state representation.

In this paper, we present a Reinforcement-Learning-based (RL) landing paradigm, where an agent learns how to safely land a multirotor on a 6-DoF landing platform without requiring explicit platform-state infor-

¹Department of Electrical and Photonics Engineering, Technical University of Denmark, Kgs. Lyngby, Denmark, ²Robotics and Perception Group, Department of Informatics, University of Zurich, Zurich

mation. To do so, the agent receives multirotor state information, containing its orientation, linear velocity and angular velocity, and images from its downward facing camera for two consecutive time steps. The method relies on sparse local features, consisting of keypoints and descriptors extracted from the platform surface in two consecutive images, to implicitly infer the relative motion of the platform with respect to the UAV. It then uses this information to predict the next commanded attitude and thrust commands. In Figure 1, a quadrotor lands autonomously on a floating platform in a pool subject to manually generated waves, using a randomly generated landing target, with all sensing and computation performed onboard.

The contributions of this paper are as follows:

- proposal of a novel method for landing a multirotor on a moving articulating platform without requiring explicit platform-state information, under minor, moderate and extreme platform motions,
- zero-shot deployment of an RL agent by designing a sparse-feature-based RL policy that can operate with different local feature extractors through a shared normalized feature interface, validated in more than 300 real-world trials,
- outperforming the state-of-the-art Model Predictive Control (MPC) method, under platform motions corresponding to conditions up to "Very Rough", as described in [6].

II. RELATED WORK

Autonomous landing is a fundamental capability for UAVs, as it directly affects mission endurance, safety, and operational autonomy. Compared with general trajectory tracking or waypoint navigation, landing requires accurate relative pose regulation close to the ground while satisfying strict constraints on touchdown lateral alignment, attitude, and velocity. These challenges become more pronounced when the landing target is moving, since the controller must not only stabilize the UAV but also synchronize its motion with the platform. Recent reviews have highlighted that autonomous drone landing remains an open problem, especially when moving platforms, environmental disturbances, and limited onboard sensing are considered [7]–[9].

Visual-servoing-based landing and tracking methods have been introduced to solve the problem of landing on moving and articulating platforms. These approaches use structured visual targets, such as AprilTags [10], ArUco markers [11] or helipad targets, to calculate the relative position and motion of the landing target to the robot. In the maritime landing setting, [12] proposes an Image-Based Visual Servoing (IBVS) controller for autonomous landing on a moving ship, combining the image feedback with a ship velocity estimation. [13]

extends this direction by integrating IBVS with an online MPC controller to maintain target visibility for the duration of the landing maneuver, and increase the robustness of the system. These works rely on structured landing targets to perform successful landings, which are limited in real-life scenarios where the visibility is limited.

Model-based and predictive-control methods aim to overcome the limitations of visual-servoing methods. Instead of relying just on visual feedback of the landing site, these methods try to predict the movement of the platform in the future time steps to generate trajectories towards successful landings and satisfy touchdown conditions. [14] proposes a nonlinear controller paired with a vision-based platform detection and estimation algorithm, to land on a horizontally moving platform. [15] uses an Euler-based MPC controller coupled with an online axis decomposition predictor of vessel movements to land a UAV on an Unmanned Surface Vehicle (USV), when the USV tilt angle is less than 5° . This work is extended by [6], that instead of opportunistically landing during the near-zero deck tilt state of the platform, an online MPC-based trajectory generation framework continuously replans trajectories based on the predicted USV poses to land faster and more robustly, utilizing fusion of sensor readings onboard the USV and UAV. These methods have achieved impressive results in simulation, and have been validated under ideal weather conditions in real world experiments, but still depend on structured landing representations and explicit platform-state prediction modules.

RL-based landing methods on moving platforms have been demonstrated in a number of works with real-world validation. The authors in [16] utilize a Deep Deterministic Policy Gradients algorithm to land a quadrotor on a vertically moving platform in simulation and real-world. In [17], a Deep Reinforcement Learning (DRL) policy is trained to land a vertical take-off and landing vehicle on a 6-DoF platform under wind disturbances, by detecting a horizon bar installed next to the landing platform. In [18], a hybrid DRL landing policy is chosen to augment a PID-based baseline with corrective feedback, to improve the landing performance on moving platforms. These methods use reinforcement learning to land UAVs on moving platforms, but do it for zero to small maximum tilt of platforms.

III. METHODOLOGY

An overview of the proposed method is shown in Figure 2. We train a sensorimotor controller that maps current and previous sparse visual observations, multirotor states, and the previous action to attitude and thrust commands. These commands are used by the low-level attitude controller of our simulated and real multirotors to land on a moving platform.

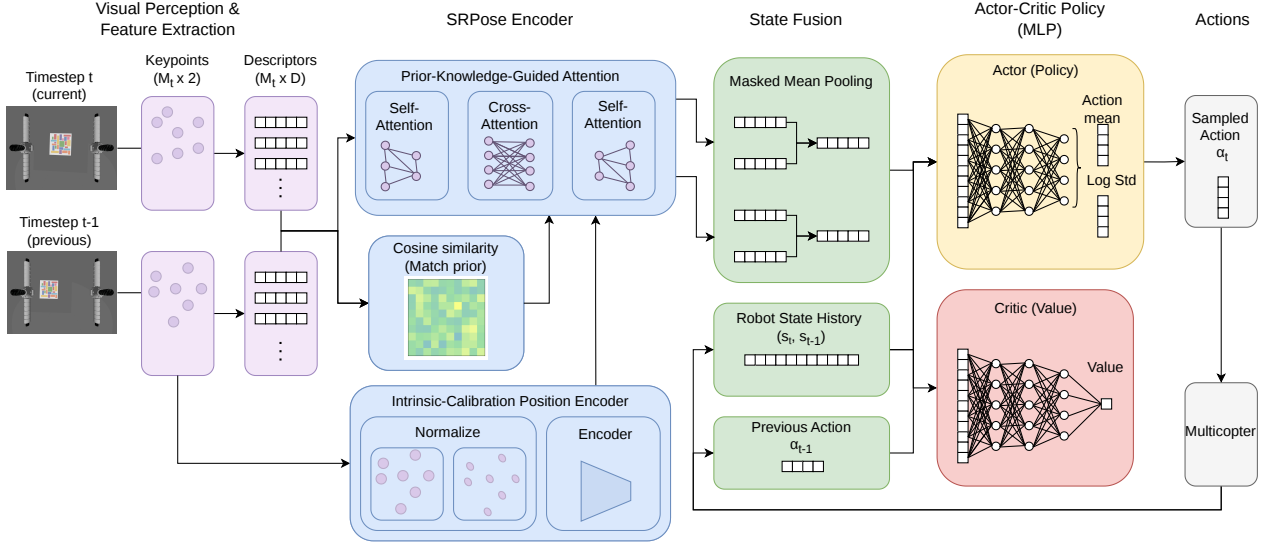


Fig. 2: Overview of the proposed approach. Sparse local features are extracted from consecutive camera images and encoded together with multirotor state history and the previous action to predict attitude and thrust commands.

A. Task Formulation

We formulate autonomous landing on a moving platform as a Partially Observable Markov Decision Process (POMDP), in which the multirotor must approach the platform, align its motion and attitude with the platform motion, and complete a controlled touchdown. Since the state of the moving platform is not directly available to the policy, the agent must infer the relative motion of the platform from onboard state measurements and temporally adjacent visual observations.

At each control step t , the policy outputs a continuous action

$$a_t = [r_t, p_t, y_t, T_t], \quad (1)$$

where r_t , p_t , and y_t denote commanded roll, pitch, and yaw, respectively, and T_t is the collective thrust command. These commands are passed to the low-level attitude controller of the multirotor, which tracks the commanded attitude and thrust.

The observation at time step t is defined as:

$$o_t = [M_t, M_{t-1}, s_t, s_{t-1}, a_{t-1}], \quad (2)$$

where M_t and M_{t-1} are sparse local features extracted from images I_t and I_{t-1} from the downward-facing camera, s_t and s_{t-1} are multirotor states, and a_{t-1} is the previous action. The state is defined as:

$$s(t) = [\mathbf{v}_t, \mathbf{q}_t, \boldsymbol{\omega}_t], \quad (3)$$

where \mathbf{v}_t is the linear velocity of the multirotor, \mathbf{q}_t is its orientation, and $\boldsymbol{\omega}_t$ is its angular velocity. Camera images and state measurements are collected at a fixed frequency.

The image observations are passed through the vision pipeline to produce a visual feature representation F_t . The policy therefore receives the concatenated vector

$$x_t = [F_t, s_t, s_{t-1}, a_{t-1}], \quad (4)$$

and predicts the next action a_t .

1) *Platform Motion Model*: In ship theory, the motion of a ship can be approximated as oscillatory motion with damping effects [19]. Based on this observation, we model the landing platform motion as sinusoidal excitation along the heave, roll, pitch, and yaw axes. For each excited DoF i , the platform motion is given by

$$\eta_i(t) = A_i \sin(2\pi f t + \phi_i), \quad (5)$$

where A_i is the motion amplitude, f is the oscillation frequency, and ϕ_i is the phase offset. The amplitudes are sampled independently for each axis, while the frequency is shared across the excited axes. This produces a set of differently oscillating landing platforms during training.

2) *Termination Conditions*: Following prior moving-platform landing works [6], [15], an episode is considered successful when the multirotor reaches the landing region with sufficiently small relative position, orientation, and velocity errors with respect to the platform. The success mask is defined as:

$$\mathbb{M}_{\text{suc}} = \begin{cases} 1, & \text{if } \begin{aligned} & d_{xy} < 1 \text{ m} \\ & \wedge \Delta p_z < 0.2 \text{ m} \\ & \wedge \Delta \theta_o < 10^\circ \\ & \wedge \Delta v < 1.5 \text{ m/s,} \end{aligned} \\ 0, & \text{otherwise,} \end{cases} \quad (6)$$

where d_{xy} is the horizontal distance, Δp_z is the absolute vertical position error, $\Delta \theta_o$ is the orientation error, and $\Delta v = \|\mathbf{v}_r - \mathbf{v}_p\|_2$ is the linear velocity error between the multirotor and the platform center.

An episode is considered failed if the multirotor moves too far away from the platform or it collides with it with excessive force. Not every contact with the platform terminates an episode. In cases where the multirotor contacts the platform with low impact force but does not satisfy the success criteria, the episode continues, allowing the multirotor to recover and attempt the landing again. The failure mask is defined as:

$$\mathbb{M}_{\text{fail}} = \begin{cases} 1, & \text{if } d_t > 10 \text{ m} \vee F_{\text{crs}} > 10 \text{ N}, \\ 0, & \text{otherwise,} \end{cases} \quad (7)$$

where d_t is the Euclidean distance between the multirotor and the platform center, and F_{crs} is the measured contact force during collision.

The episode terminates when either $\mathbb{M}_{\text{suc}} = 1$, $\mathbb{M}_{\text{fail}} = 1$, or when the episode reaches the maximum horizon T_{max} . Episodes that reach T_{max} without satisfying either terminal condition are counted as timeouts.

3) *Reward shaping*: The reward function consists of dense shaping terms and terminal terms. The dense terms encourage the multirotor to approach the platform, maintain useful visual observations, reduce relative motion errors, and avoid unsafe configurations. The terminal terms reward successful landings and penalize failed attempts. The reward parameter values used during training are listed in Table I.

The total reward at time step t is

$$\mathcal{R}_t = r_t^{\text{app}} + r_t^{\text{perc}} + r_t^{\text{smooth}} + r_t^{\text{pos}} r_t^{\text{align}} + r_t^{\text{term}}, \quad (8)$$

where r_t^{app} is the approach reward, r_t^{perc} is the perception reward, r_t^{smooth} penalizes abrupt commands, r_t^{align} rewards velocity and attitude alignment near the platform, r_t^{pos} acts as a proximity gate, and r_t^{term} contains the terminal success and failure rewards.

a) *Approach reward*: The approach reward encourages progress toward the platform:

$$r_t^{\text{app}} = r_t^{\text{prog}} + r_t^{\text{vd}}, \quad (9)$$

where

$$r_t^{\text{prog}} = \lambda_1 (d_{t-1} - d_t), \quad (10)$$

$$r_t^{\text{vd}} = \lambda_2 e^{-\lambda_3 \theta_v^2}. \quad (11)$$

Here, θ_v is the angle between the multirotor velocity vector and the direction vector from the multirotor to the platform center. The r_t^{prog} term rewards reduction in distance, while the r_t^{vd} term encourages the velocity direction to point toward the platform center.

b) *Perception reward*: To keep the landing platform inside the camera field of view, we reward alignment between the camera optical axis and the platform center:

$$r_t^{\text{perc}} = \lambda_4 e^{-\lambda_5 \theta_c^2}, \quad (12)$$

where θ_c is the angle between the optical axis of the downward-facing camera and the direction vector from the camera to the platform center.

c) *Command smoothness penalty*: To discourage aggressive changes in the commanded attitude and thrust, we penalize action differences between consecutive time steps:

$$r_t^{\text{smooth}} = \lambda_6 \|a_t - a_{t-1}\|_2 c_t, \quad (13)$$

where $\lambda_6 < 0$ and c_t is the curriculum progress factor. This penalty becomes more influential as the curriculum progresses.

d) *Near-platform alignment reward*: Once the multirotor approaches the platform, the policy is encouraged to match the platform velocity and orientation. This is achieved using:

$$r_t^{\text{align}} = r_t^{\text{lv}} + r_t^{\text{or}} + r_t^{\text{col}}, \quad (14)$$

where

$$r_t^{\text{lv}} = \lambda_7 e^{-\lambda_8 \Delta v^2}, \quad (15)$$

$$r_t^{\text{or}} = \lambda_9 e^{-\lambda_{10} \Delta \theta_o^2}, \quad (16)$$

$$r_t^{\text{col}} = \lambda_{11} \min((|\Delta p_z| + \Delta p_z) \cos \Delta \theta_o - \lambda_{12}, 0). \quad (17)$$

Here, Δv is the linear velocity error between the multirotor and the platform, $\Delta \theta_o$ is the orientation error between the thrust vector and the platform normal vector, and Δp_z is the vertical position error. The collision-avoidance term penalizes configurations in which the multirotor is close to the platform while being poorly aligned, which could result in propeller-platform contact.

The alignment reward is multiplied by a proximity term:

$$r_t^{\text{pos}} = e^{-\lambda_{13} d_t^2}. \quad (18)$$

This ensures that precise velocity and orientation matching are emphasized primarily when the multirotor is close to the landing platform.

e) *Terminal reward*: The terminal reward consists of a success bonus and a failure penalty:

$$r_t^{\text{term}} = r_t^{\text{suc}} + r_t^{\text{fail}}, \quad (19)$$

where

$$r_t^{\text{suc}} = \mathbb{M}_{\text{suc}} \left(\lambda_{14} \frac{T_{\text{max}} - t}{T_{\text{max}}} + \lambda_{15} (T_{\text{max}} - t) \right), \quad (20)$$

$$r_t^{\text{fail}} = \lambda_{16} \mathbb{M}_{\text{fail}}. \quad (21)$$

The success reward is scaled by the remaining episode time, encouraging the agent to complete the landing efficiently rather than hovering near the platform. The failure term penalizes crashes and out-of-bounds states.

TABLE I: Reward-function parameter values.

Param.	Value	Param.	Value
λ_1	1e0	λ_9	1e-1
λ_2	5e-2	λ_{10}	1e1
λ_3	5e0	λ_{11}	1e-1
λ_4	2e-2	λ_{12}	2e-1
λ_5	1e1	λ_{13}	5e-1
λ_6	-1e-1	λ_{14}	1e1
λ_7	2e-2	λ_{15}	2e-2
λ_8	5e0	λ_{16}	1e0

B. Vision pipeline

To improve robustness to visual domain shift, we provide the policy with a sparse visual-feature representation rather than raw RGB images. Instead of using segmentation masks as input to our network as prior works do [20]–[22], we use sparse local features. We use the term sparse local features to refer to keypoint coordinates together with their associated descriptors. Segmentation-based representations can be sensitive to boundary quality, illumination, and appearance changes between simulation and real maritime scenes. Sparse local features provide a lower-dimensional abstraction that emphasizes repeatable local structure rather than dense appearance.

SRPose [23] provides a sparse keypoint-based encoder for two-view relative pose estimation. We adopt the SRPose encoder as the visual abstraction module for our policy, with the modification that all descriptors are L2-normalized before being processed by the network. At each time step t , sparse keypoints and descriptors are extracted from the current and previous images, I_t and I_{t-1} . The keypoint coordinates are normalized using the camera intrinsics, while the descriptors are L2-normalized so that the cosine-similarity depends on descriptor direction rather than descriptor magnitude.

The normalized descriptors are used to construct a match prior between the two views, and the normalized keypoint coordinates are passed through the position encoder to obtain positional embeddings. The resulting descriptor and positional representations are processed by the SRPose attention encoder, which combines self-attention within each image with prior-knowledge-guided cross-attention across the two images. This produces a compact feature representation that captures implicit correspondences between temporally adjacent observations. The resulting visual feature vector F_t is then provided to the policy network, allowing the policy to infer relative motion cues between the multirotor and the landing platform without requiring platform-state estimation or prediction.

L2 normalization provides a common descriptor interface across training and deployment and facilitates transfer between local feature extractors. During deployment, the local feature extractor must produce descriptor vectors with the same dimensionality as those used during training, which we normalize before passing to the

TABLE II: PPO training hyperparameters.

Parameter	Value	Parameter	Value
Total time steps	10^8	Rollout steps	256
Mini-batches	16	Update epochs	1
Learning rate	3×10^{-4}	Optimizer	Adam
Discount γ	0.98	GAE λ	0.95
Clip coefficient	0.2	Entropy coeff.	10^{-3}
Value-loss coeff.	2.0	Max grad. norm	1.0

SRPose encoder. In this formulation, the descriptors are used to define correspondence priors between keypoints across images, rather than to provide visual or semantic appearance information to the control policy. This decouples the control policy from raw image appearance and reduces the vision-induced sim-to-real gap, while still allowing different local feature extractors to be used within the same sparse-feature interface.

C. Policy

The policy is implemented as a Gaussian actor-critic architecture with separate MLPs for the actor and critic. On each time step t , both networks receive the concatenated input x_t . The actor outputs the mean of a Gaussian action distribution, while the critic outputs a scalar value estimate. Both networks are two-layer MLPs with 512 hidden units per layer and tanh activations. No privileged information is provided to the critic.

D. Training details

We conduct training experiments in Aerial Gym [24], a highly parallelized GPU-based simulator for aerial vehicles built on NVIDIA Isaac Gym. This enables us to run multiple episodes simultaneously, reducing the time needed for training. The SRPose encoder, policy network, and value network are trained jointly using PPO [25], with the output of the image-based local feature extraction module replaced by synthetic projected platform features. The PPO hyperparameters are listed in Table II.

To support transfer to the real multirotor, we model the vehicle in simulation and tune its low-level attitude and thrust response to match the real platform response to commanded actions. At the beginning of each episode, the multirotor is initialized above the landing platform such that the platform is fully or partially visible from the downward-facing camera. The camera pose is randomized within small perturbation bounds to improve robustness to extrinsic calibration errors.

At the beginning of each episode, the platform is initialized at a fixed nominal position. The amplitudes of the heave, roll, pitch, and yaw motions are sampled from uniform distributions, with roll and pitch sampled from $[-\pi/6, \pi/6]$ rad, yaw from $[-\pi/16, \pi/16]$ rad, and heave from $[0.0, 5.0]$ m. A single oscillation frequency is sampled from $[0, 0.5]$ Hz at the beginning of each episode and shared across all excited degrees of freedom.

TABLE III: Simulation results for different landing methods.

Method	Success (%)	Crash (%)	Timeout (%)	AMT (s)
MPC-NE	46.69	35.93	17.38	86.22
Ours (PD)	72.14	27.86	0.0	2.33
Ours (RD)	61.20	38.80	0.0	5.61

These ranges are chosen to cover scenarios up to “Very Rough” sea conditions, as characterized in [6], thereby exposing the policy to a diverse set of platform motions during training.

We use curriculum learning to improve training stability and sample efficiency. Training begins with a static landing platform. Once the success rate exceeds 90%, roll, pitch, and yaw amplitudes and frequencies are sampled from the predefined ranges, while the maximum heave amplitude is kept at 0 m. Subsequently, if the success rate over the previous 4096 episodes exceeds 60%, the maximum heave amplitude is increased by 0.5 m. If the success rate falls below 20%, the maximum heave amplitude is decreased by 0.25 m. At the hardest curriculum level, the maximum heave amplitude is capped at 5 m.

For each episode, 25 points are sampled on the platform surface using a uniform distribution. Each point is assigned a fixed 64-dimensional descriptor vector sampled from a normal distribution. At each time step, the visible points are projected into the camera frame and used as sparse local-feature observations. To emulate imperfect feature extraction, 20% of the descriptors are randomly dropped at each time step, and noise is added to the remaining descriptors. This randomization encourages robustness to missing features, descriptor noise, and changes in the deployment local feature extractor.

To account for sensor uncertainty during deployment, noise is added to the multirotor state observations during training. Specifically, noise is applied to the measured linear velocity, attitude, and angular velocity at each time step. This improves the robustness of the learned policy to noisy onboard state estimates.

IV. EXPERIMENTS

We evaluate the proposed method in both a ROS-based Gazebo simulation environment and real-world experiments. The deployment pipeline consists of three components: landing-platform detection, sparse local feature extraction, and the trained landing policy. The UAV employs the PX4 controller stack, and the communication between the policy and the low-level controller is handled through ROS2.

A. Experiments in Simulations

We first evaluate the proposed method in a realistic ROS-based Gazebo simulation environment. We compare against MPC-NE [15], a state-of-the-art moving-platform landing method for multirotors. MPC-NE uses

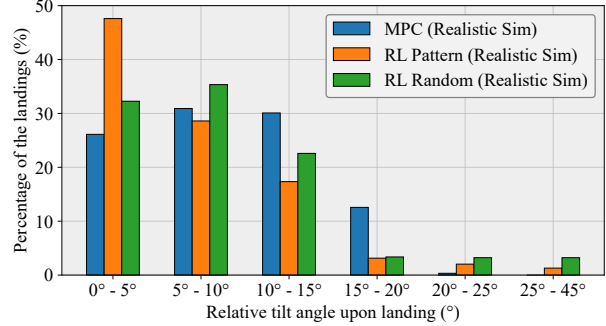


Fig. 3: Histogram comparison between the proposed approach and the baseline approach during the touchdown of the UAV on the USV deck. Higher concentration on the left side of the figure indicates better performance.

fiducial markers placed on the landing platform to detect and predict the platform motion. To separate the effect of the visual target representation from the landing policy, we evaluate two variants of the proposed method: one using a predefined AprilTag-based feature layout and one using a randomly generated visual pattern on the landing platform.

In the predefined-descriptor setting, denoted as Ours (PD), the policy is trained using 25 uniformly distributed points arranged in a symmetric 5×5 pattern. Each point is associated with a predefined randomly generated descriptor. During deployment, an AprilTag detector is used to localize the tag on the landing platform, and the same 5×5 keypoint layout and descriptor assignment used during training are applied to the detected tag region. The resulting keypoint-descriptor pairs are then passed to the policy for inference.

In the random-descriptor setting, denoted as Ours (RD), the policy is trained as described in Section III, using randomly generated keypoints and descriptors. During testing, the landing-platform region is detected, and A-KAZE [26] is used to extract keypoint-descriptor pairs from the randomly generated visual pattern on the platform. The 25 keypoints with the highest detector response are selected and passed to the policy.

For the simulation evaluation, we perform 500 landing trials for each method. For each method, 100 trials are conducted at each platform oscillation frequency in the range $[0.1, 0.5]$ Hz, with a step size of 0.1 Hz. For every trial, the amplitudes of the platform motion are sampled randomly within the maximum ranges defined in Section III-D. Figure 3 shows the distribution of the relative touchdown angle between the multirotor and the platform, following the evaluation style of [15]. A higher concentration at low angles indicates better alignment during touchdown.

While the touchdown-angle distribution provides insight into attitude alignment at contact, it does not

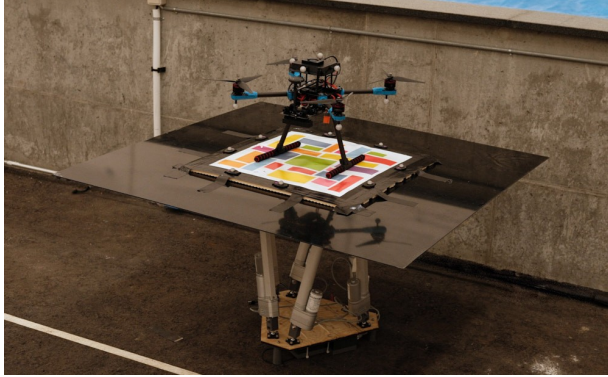


Fig. 4: Illustration of quadrotor and 6-DoF Stewart Platform used for experiments. The pattern on top of the landing platform is randomly generated and not seen during training.

fully characterize landing quality because it does not account for the relative touchdown velocity or relative position. Therefore, we additionally report Success rate, Crash rate, Timeout rate, and Average Maneuver Time (AMT) in Table III. Success is evaluated using the criteria defined in Equation 6. For MPC-NE, we exclude the estimator convergence time and measure only the landing maneuver time. A trial is counted as a timeout if the landing maneuver does not terminate within 2 minutes after the MPC-NE filter has converged. AMT is computed over trials that terminate in either success or crash.

Table III shows that Ours (PD) achieves the highest success rate, the lowest crash rate, no timeouts, and the shortest maneuver time. Compared with MPC-NE, Ours (PD) improves the success rate by 25.45 percentage points and reduces AMT by approximately $37\times$. Ours (RD) also improves the success rate by 14.51 percentage points and eliminates timeouts, while reducing AMT by approximately $15.4\times$. However, Ours (RD) has a slightly higher crash rate than MPC-NE, indicating that the random-feature setting is more challenging than the predefined-descriptor setting. Overall, the results indicate that the proposed policy enables faster and more successful landings than MPC-NE under the evaluated simulation conditions, particularly when using the predefined sparse-feature interface.

B. Deployment in the Real World

We further validate the proposed method through real-world landing experiments. The complete deployment pipeline runs onboard a custom quadrotor equipped with a Jetson Orin Nano. An object detection module first localizes the landing-platform region in the downward-facing camera image. Sparse local features are then extracted inside the detected region using either A-KAZE or SURF [27]. For both methods, we use non-extended

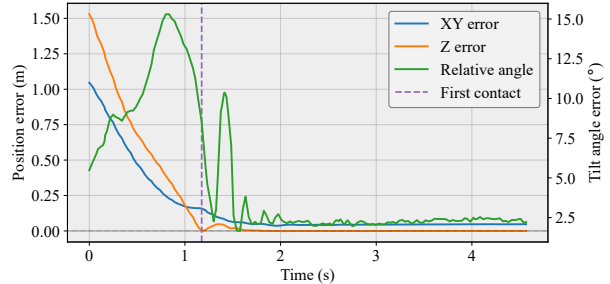


Fig. 5: Representative successful landing during the qualitative floating-platform pool demonstration.

TABLE IV: Real-world experiment results.

Success (%)	Tilt angle violation (%)	Velocity violation (%)	AMT (s)
58.38	40.5	4.19	4.24

64-dimensional descriptors. The 25 features with the highest detector response are selected and passed to the trained policy, which predicts attitude and thrust commands. These commands are tracked by the tuned PX4 low-level controller. The policy communicates with PX4 through ROS2 and runs at 30 Hz.

During deployment, we switch between A-KAZE and SURF while using the same trained policy. This evaluates whether the policy can operate with multiple local feature extractors through the shared sparse-feature interface, without policy retraining.

We first evaluate the method using a 6-DoF Stewart platform [28] with a randomly generated visual pattern attached to the landing pad. We perform 358 landing trials with the platform oscillating in roll and heave at 0.2 Hz. The maximum roll and heave amplitudes are 20° and 0.25 m, respectively. Table IV reports the real-world deployment results using this setup. The evaluation criteria are the same as those used in simulation. Most failed trials violate the touchdown tilt-angle criterion rather than the velocity criterion. In these cases, the vehicle often remains on the platform after contact instead of rebounding or crashing. Thus, the reported success rate reflects strict satisfaction of the touchdown criteria at the instant of contact, rather than post-contact recoverability.

Finally, we provide a qualitative demonstration using the same landing pad mounted on a floating platform in a pool, where manually generated waves induce platform motion, as shown in Figure 1. In these experiments, the same onboard perception-control pipeline used in the Stewart-platform experiments was deployed without retraining. The purpose of this evaluation is to assess qualitative transfer to wave-induced floating-platform motion, which produces irregular platform dynamics that differ from the sinusoidal motion model used during training. Figure 5 shows the relative position and attitude during a representative landing trial. A small rebound is observed after initial contact, but the relative attitude

remains below 10° throughout the post-contact motion.

V. CONCLUSION

This paper presented a reinforcement-learning-based approach for autonomous multirotor landing on moving maritime platforms. The proposed method uses sparse local features together with multirotor state information to directly predict attitude and thrust commands that can be tracked by a conventional attitude controller. The simulation experiments demonstrated that the proposed method outperforms the MPC-NE baseline in both success rate and average maneuver time, for sea conditions up to "Very Rough", based on the classification in [6]. Furthermore, the real-world experiments validated that the same policy can be deployed zero-shot with different local feature extractors and can run onboard a UAV without external sensing, external computation, or explicit platform-state information.

REFERENCES

- [1] P. Doherty and P. Rudol, "A UAV Search and Rescue Scenario with Human Body Detection and Geolocalization," in *AI 2007: Advances in Artificial Intelligence*, M. A. Orgun and J. Thornton, Eds. Berlin, Heidelberg: Springer, 2007, pp. 1–13.
- [2] V. A. Feraru, R. E. Andersen, and E. Boukas, "Towards an Autonomous UAV-based System to Assist Search and Rescue Operations in Man Overboard Incidents," in *2020 IEEE International Symposium on Safety, Security, and Rescue Robotics (SSRR)*, November 2020, pp. 57–64, iSSN: 2475-8426.
- [3] D. Angelis, R. E. Andersen, V. A. Feraru, and E. Boukas, "UAV Design for Fully Autonomous Man Overboard Detection," in *2024 IEEE International Conference on Imaging Systems and Techniques (IST)*, October 2024, pp. 1–6.
- [4] J. Fortuna, F. Ferreira, R. Gomes, S. Ferreira, and J. Sousa, "Using low cost open source UAVs for marine wild life monitoring - Field Report*," *IFAC Proceedings Volumes*, vol. 46, no. 30, pp. 291–295, January 2013.
- [5] M. Peti, L. Marković, I. Lončar, A. Barišić Kulaš, F. Petric, A. Milas, J. Goričanec, M. Car, M. Orsag, B. A. Ferreira, and S. Bogdan, "Aerial Localization and Navigation for Surveillance of Large, Featureless, GNSS-Denied Maritime Environments," *Journal of Field Robotics*, vol. 42, no. 8, pp. 4215–4235, 2025, eprint: <https://onlinelibrary.wiley.com/doi/pdf/10.1002/rob.22610>.
- [6] O. Procházka, F. Novák, T. Báča, P. M. Gupta, R. Pěnička, and M. Saska, "Model predictive control-based trajectory generation for agile landing of unmanned aerial vehicle on a moving boat," *Ocean Engineering*, vol. 313, p. 119164, December 2024, arXiv:2412.07332 [cs].
- [7] L. Xin, Z. Tang, W. Gai, and H. Liu, "Vision-Based Autonomous Landing for the UAV: A Review," *Aerospace*, vol. 9, no. 11, p. 634, November 2022.
- [8] L. G. Leandro de Paula, V. S. Dwivedi, H.-S. Shin, and A. Tsourdos, "A Review on VTOL Autonomous Landing Strategies on Naval Dynamic Surfaces," p. 30 pages, June 2022, artwork Size: 30 pages Medium: application/pdf Version Number: 1.0.
- [9] J. Amendola, L. R. Cenkeramaddi, and A. Jha, "Drone Landing and Reinforcement Learning: State-of-Art, Challenges and Opportunities," *IEEE Open Journal of Intelligent Transportation Systems*, vol. 5, pp. 520–539, 2024.
- [10] E. Olson, "AprilTag: A robust and flexible visual fiducial system," in *2011 IEEE International Conference on Robotics and Automation*, May 2011, pp. 3400–3407, iSSN: 1050-4729.
- [11] S. Garrido-Jurado, R. Muñoz-Salinas, F. J. Madrid-Cuevas, and M. J. Marín-Jiménez, "Automatic generation and detection of highly reliable fiducial markers under occlusion," *Pattern Recognition*, vol. 47, no. 6, pp. 2280–2292, June 2014.
- [12] G. Cho, J. Choi, G. Bae, and H. Oh, "Autonomous ship deck landing of a quadrotor UAV using feed-forward image-based visual servoing," *Aerospace Science and Technology*, vol. 130, p. 107869, November 2022.
- [13] L. Yang, X. Wang, Z. Liu, and L. Shen, "Robust Online Predictive Visual Servoing for Autonomous Landing of a Rotor UAV," *IEEE Transactions on Intelligent Vehicles*, vol. 10, no. 4, pp. 2818–2835, April 2025.
- [14] D. Falanga, A. Zanchettin, A. Simovic, J. Delmerico, and D. Scaramuzza, "Vision-based autonomous quadrotor landing on a moving platform," in *2017 IEEE International Symposium on Safety, Security and Rescue Robotics (SSRR)*, October 2017, pp. 200–207, iSSN: 2475-8426.
- [15] P. M. Gupta, E. Pairet, T. Nascimento, and M. Saska, "Landing a UAV in Harsh Winds and Turbulent Open Waters," *IEEE Robotics and Automation Letters*, vol. 8, no. 2, pp. 744–751, February 2023.
- [16] A. Rodriguez-Ramos, C. Sampedro, H. Bavlé, P. de la Puente, and P. Campoy, "A deep reinforcement learning strategy for uav autonomous landing on a moving platform," *Journal of Intelligent & Robotic Systems*, vol. 93, pp. 351–366, 2019.
- [17] B. Lee, V. Saj, D. Kalathil, and M. Benedict, "A deep reinforcement learning control strategy for vision-based ship landing of vertical flight aircraft," in *AIAA AVIATION 2021 FORUM*, 2021.
- [18] L. Wu, C. Wang, P. Zhang, and C. Wei, "Deep reinforcement learning with corrective feedback for autonomous uav landing on a mobile platform," *Drones*, vol. 6, no. 9, p. 238, 2022.
- [19] S.-K. Ueng, D. Lin, and C.-H. Liu, "A ship motion simulation system," *Virtual Reality*, vol. 12, no. 1, pp. 65–76, March 2008.
- [20] L. Bartolomei, L. Teixeira, and M. Chli, "Semantic-aware Active Perception for UAVs using Deep Reinforcement Learning," in *2021 IEEE/RSJ International Conference on Intelligent Robots and Systems (IROS)*. Prague, Czech Republic: IEEE, September 2021, pp. 3101–3108.
- [21] E. Kaufmann, L. Bauersfeld, A. Loquercio, M. Müller, V. Koltun, and D. Scaramuzza, "Champion-level drone racing using deep reinforcement learning," *Nature*, vol. 620, no. 7976, pp. 982–987, August 2023.
- [22] I. Geles, L. Bauersfeld, A. Romero, J. Xing, and D. Scaramuzza, "Demonstrating Agile Flight from Pixels without State Estimation," June 2024, arXiv:2406.12505 [cs].
- [23] R. Yin, Y. Zhang, Z. Pan, J. Zhu, C. Wang, and B. Jia, "SRPose: Two-View Relative Pose Estimation with Sparse Keypoints," in *Computer Vision - ECCV 2024*, A. Leonardis, E. Ricci, S. Roth, O. Russakovsky, T. Sattler, and G. Varol, Eds. Cham: Springer Nature Switzerland, 2025, pp. 88–107.
- [24] M. Kulkarni, W. Rehberg, and K. Alexis, "Aerial gym simulator: A framework for highly parallelized simulation of aerial robots," *IEEE Robotics and Automation Letters*, vol. 10, no. 4, pp. 4093–4100, 2025.
- [25] J. Schulman, F. Wolski, P. Dhariwal, A. Radford, and O. Klimov, "Proximal Policy Optimization Algorithms," August 2017, arXiv:1707.06347 [cs].
- [26] P. Alcantarilla, J. Nuevo, and A. Bartoli, "Fast Explicit Diffusion for Accelerated Features in Nonlinear Scale Spaces," in *Proceedings of the British Machine Vision Conference 2013*. Bristol: British Machine Vision Association, 2013, pp. 13.1–13.11.
- [27] H. Bay, A. Ess, T. Tuytelaars, and L. Van Gool, "Speeded-Up Robust Features (SURF)," *Computer Vision and Image Understanding*, vol. 110, no. 3, pp. 346–359, June 2008.
- [28] D. Stewart, "A Platform with Six Degrees of Freedom," *Proceedings of the Institution of Mechanical Engineers*, vol. 180, no. 1, pp. 371–386, June 1965.